54th CIRP Conference on Manufacturing Systems

Influence of Part Geometry and Feature Size on the Resulting Microstructure and Mechanical Properties of the Case Hardening Steel 16MnCr5 processed by Laser Powder Bed Fusion

Matthias Schmitt[a],*, Florian Gerstl[a], Max Boesele[a], Max Horn[a], Georg Schlick[a], Johannes Schilp[a,b], Gunther Reinhart[a,c]

[a]*Fraunhofer-Institute for Casting, Composite and Processing Technology IGCV, Am Technologiezentrum 10, D-,86159 Augsburg, Germany*
[b]*University of Augsburg, Chair of Digital Manufacturing, Faculty of Applied Computer Sience, Eichleitnerstr. 30, D-86159 Augsburg, Germany*
[c]*Institute for Machine Tools and Industrial Management (iwb), Technical University of Munich, D-85748 Garching, Germany*

* Corresponding author. Tel.: +49 821 90 678 147. Fax: +49 821 90 678 199. *Email address:* matthias.schmitt@igcv.fraunhofer.de;

Abstract

Additive manufacturing, especially laser powder bed fusion (LPBF), allows the build-up of complex parts. However, the resulting microstructure is not only influenced by the manufacturing parameters but also by the part geometry due to the influence on heat dissipation. At first, six geometric features are identified which can affect heat dissipation. Geometric samples of a case-hardening steel are produced via LPBF. Analysis of the microstructure and the mechanical properties show that the cross-sectional area and overhang angles have significant influence resulting in a hardness differences of more than 90 HV while increasing the ferrite content with increasing overhang angles. For further investigation, the results are analytically linked to the part density.

Keywords: case-hardening steel, 16MnCr5, influence of geometry, microstructure, heat dissipation

1. Introduction

Additive manufacturing technologies are characterized by a build-up in layers, which gives great freedom in part designs that include lightweight structures (e.g. lattice) or integrated cooling channels [1]. With the given opportunities, new part designs and business models are evolving that include spare part supply and individualization [2]. Laser powder bed fusion (LPBF) is an additive manufacturing technology whereby metal alloy powder is melted by a laser in subsequent layers, with the possibility of reaching high part density. Common metals processed by LPBF include corrosion resistant or tool steels, nickel base alloys, titanium alloys and aluminum alloys [3]. One commonly used group of materials in the automotive industry are case-hardening steels, which are applied in complex and highly loaded drivetrain parts e.g. gears, shafts and shift forks. Case-hardening steels possess a carbon content of around 0.15-0.23 weight-% and their use in additive manufacturing has only recently become the focus of research [4,5]. Beer et al. investigated process conditions for the case-hardening steel M50NiL, with emphasis on the shielding gas flow [6]. Case-hardening properties were investigated by Bartels et al. showing differences in carbon diffusion and resulting case-hardening depth [7].

In contrast to cutting processes, LPBF does not only form the part geometry but also defines the microstructure of the part [8]. The formation of the microstructure in LPBF is a complex procedure with many variables and is strongly influenced by factors alternating the heat dissipation in the cooling phase [9] Studies carried out so far focus on the relation between process

variables (e.g. laser parameters, baseplate heating, scan vectors) and the resulting microstructure [10]. In contrast, the influence of the part geometry on the resulting heat dissipation and therefore on the microstructure is neglected and only a few studies are available. Mohr et al. investigated the effect of the part height on the resulting microstructure showing that the heat accumulation in parts built from 316L lead to a decreased hardness in the upper part of tall specimens [11]. Additionally, the feature size can be an important parameter in the resulting microstructure of Ti-6Al-4V. Furthermore, the porosity of the features increased significantly (from 0.3 to 4.77%) with decreasing feature size [12]. Increased porosity for small feature sizes was also observed for AlSi10Mg [13]. Altering the heat dissipation of the tensile specimen through removable heat sinks leads to a significantly improved ductility of a binary Fe-50Co alloy [14]. The investigations show that geometry can play a large, previously underestimated role and that inhomogeneous material properties can be expected over a complex part geometry. Further challenges arise through varying structure diameters in topology optimized parts or parts including lattices. Here, a size dependent effect is observed and the strength changes with the feature size [15]. Up to now, these changing properties are not taken into account during part design (e.g. through finite element analysis, FEA). This leads to uncertainties and parts with excessive safety factors opposing lightweight design principles. In the following, general geometric principles possibly influencing the heat dissipation are derived and the effect for the case-hardening steel 16MnCr5 are determined. Furthermore, mechanical properties depending on the feature size are derived and connected to the part density by applying the Bal'shin law [16].

1.1. Case-hardening steel 16MnCr5

16MnCr5 (1.7131) is a low alloyed steel with case-hardening capabilities and is widely used in drivetrain parts such as gears and is increasingly used in LPBF [5]. The chemical composition of the powder is shown in Table 1. Particle size distribution is of approximately normal distribution, with a D10 of 28 µm, D50 of 47 µm and D90 of 72 µm.

Table 1 Chemical composition of 16MnCr5 in % by mass 1) DIN EN10084 2) supplier certificate

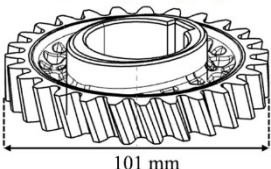|	C	Mn	Cr	Si	P	S	Fe
1)	0.14-0.19	1.0-1.3	0.8-1.1	≤ 0.4	≤ 0.025	≤ 0.035	bal.
2)	0.15	1.05	0.9	0.19	-	-	bal.

1.2. Methods and approach

To manufacture the specimens, an EOS M 290 machine was used applying a baseplate preheating of 80 °C and argon as shielding gas. Recoating took place with a carbon brush to minimize the risk of process interruptions. A layer thickness of 30 µm was chosen and the specimens were built with laser parameters derived from [5]. Particle size distribution was analyzed by laser diffraction with a Mastersizer 3000. The density was measured with the Archimedes principle using a

fine scale with a precision of 0.001 g. Microsections were generated using a grinding and polishing device (SAPHIR 530) followed by an analysis with an Olympus BX53M. Microstructure images were taken after ten seconds of etching with 5% nitric acid (5% HNO3). Hardness measurements were carried out with a Zwick Roell ZHUZ2.5 machine according to DIN EN ISO 6507-1. Hardness was measured on three specimens and the mean value of at least five measurements is depicted. Tensile tests were carried out using a Zwick Roell Z050 according to DIN EN ISO 6892-1 with five specimens per variation. Characterization of the fracture surfaces were carried out with a Hitachi TM3030Plus Tabletop scanning electron microscope (SEM).

2. Identification and selection of features

At first, the component at hand is analyzed and split into distinctive geometric features. This process can be performed by an experienced AM engineer or through utilization of a computer-aided process like feature recognition. As a use case, a lightweight optimized gear is being used. Through bionic design the part mass was reduced by 45% [17]. The part features struts with diameters from 2 to 5 mm, various overhangs of up to 30° and is built on support structure (c.f. Figure 1). As a next step, these identified features are clustered in generalized geometric features which can affect the parts' heat dissipation and therefore the resulting microstructure.

Fig. 1. AM-lightweight gear with distinguishable geometric features

Additionally, further parameters such as build job layout are considered. In summary, six principles, displayed in Figure 2, could be identified which possibly affect the parts' microstructure formation and are described in the following list:
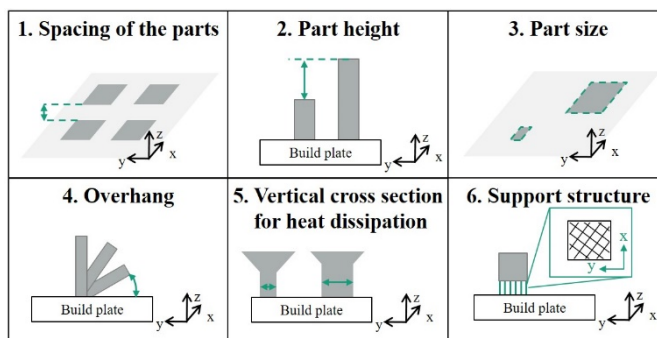

Fig. 2. Generalized principles affecting parts microstructure formation

1. The spacing of the parts since small distances between parts have the ability to accumulate heat.
2. The part height itself since during the build process a heat accumulation occurs through repeated solidification of subsequent layers. The focus here is on the effect on small parts with a part height under 15 mm, which have not been considered in the literature.
3. The solidified area of the part since this influences the number of scan tracks and therefor the energy input per layer.
4. The geometric overhang angle due to the increased amount of powder under the exposed surface with increasing overhang angle since loose powder possesses a different heat dissipation.
5. The variation of vertical cross section available for the heat dissipation to the build plate.
6. The layout of the applied support structure since lattice density increases the volume of available material for heat dissipation.

Process parameter, base plate heating and interlayer time variations are not considered since thorough studies describe these effects [10,11]. The aim of the experiments carried out in the next section is to determine and quantify the effect of the principles shown.

The next part of the experimental investigation focuses on the mechanical behavior of varied feature sizes. Therefore, round, and flat tensile specimens were built in vertical build direction (z-direction) and testing was conducted in the as-built condition without further post-processing. The feature size is in a range from 0.5 to 5 mm in diameter for the round tensile specimens and 0.5 to 5 mm in thickness for the flat tensile specimens (c.f. Figure 3). The condition of the specimens mimic the condition of a complex lightweight or a lattice structure where no post-processing is possible. The aim of the experiments carried out is to determine the tensile strength in dependency of the feature size and create a relationship between the part densities.
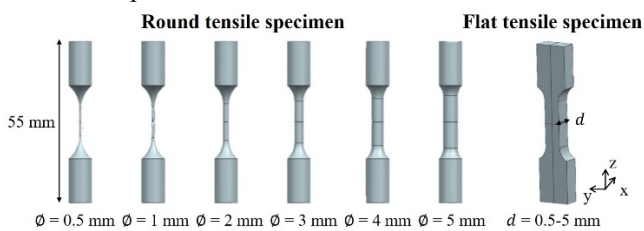

Fig. 3. Variation of the diameter of the round tensile specimens and variation of part thickness of the flat tensile specimens

3. Microstructural analysis of geometric features

To determine the effect of the part spacing's L-shaped specimens were designed and nested on the build plate within a distance s of 0.1 mm to 10 mm. Microstructure analysis and hardness measurements were conducted at the core of the specimens to determine the effect of the distance s on the part's properties. The resulting microstructure and hardness measurements are depicted in Figure 4. The microstructure shows a slight increase in ferrite content at 0.1 mm spacing distance compared to the microstructure at 10 mm spacing

distance, which is mainly composed from bainite and some martensite. However, the increase in ferrite does not lead to a significant decrease in hardness. Overall, the part's core hardness is not affected by the parts spacing distance.
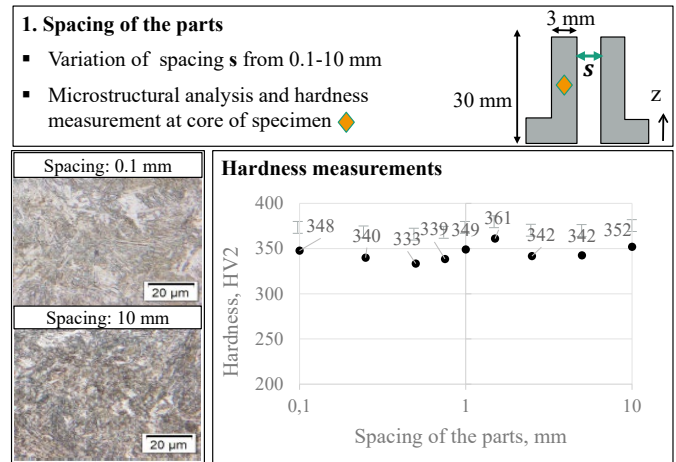

Fig. 4. Part properties in dependency of the part spacing showing no significant effect of the spacing distance on the part hardness

The effect of the part height is determined by examining the microstructure and hardness in the top section of specimens (1 mm below the surface). The part height is varied from 3 to 15 mm since the effect on taller parts was already determined by Mohr et al. [11]. The microstructure shows a high content of martensite in the small parts (height < 6 mm) and an increasing ferrite content with increasing part height. Additionally, grain coarsening is seen. The hardness measurements confirm the increasing ferrite content since the hardness decreases continuously with the part height (c.f. Figure 5). The results indicate that the heat accumulation through solidification of subsequent layers already plays a role in small parts and close to the build plate.
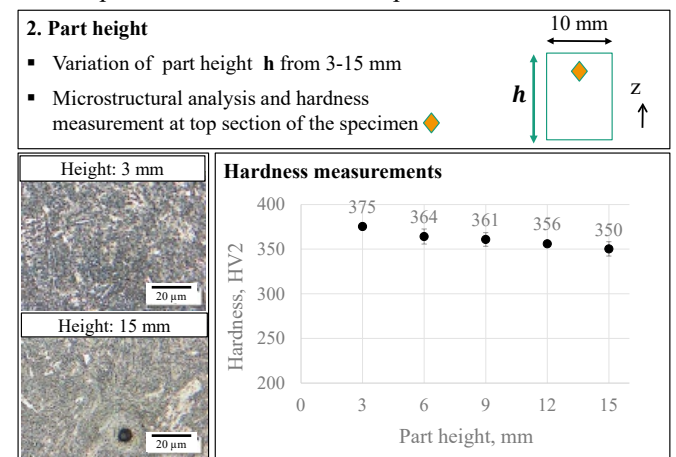

Fig. 5. Part properties in dependency of the part height showing an effect of decreasing hardness with increasing part height

In the next step, the part thickness t of wall structures with a constant part distance of 3 mm is varied from 0.3 to 3 mm. Microstructure analysis, the specimen's density and hardness measurements at the specimen's core are depicted in Figure 6. In contrast to the literature about titanium and aluminum alloys, no correlation of the density and part thickness is obvious. All

measured densities are above 99.5% relative density and no clear trend is visible with decreasing part thickness. However, standard deviation increases with decreasing part thickness. The hardness measurement ranges from 280 to 320 HV0.5 with higher hardness at higher part thickness. However, the gradient of the hardness increase is low and only little difference in ferrite content is detectable. Nevertheless, higher heat dissipation at increased part thickness leads to less ferrite formation and therefore higher part hardness.

3. Part size
- Variation of part thickness **t** from 0.3-3 mm
- Microstructural analysis, density measurement and hardness measurement at core ◆

Thickness: 0.3 mm
Thickness: 3.0 mm

Hardness measurements
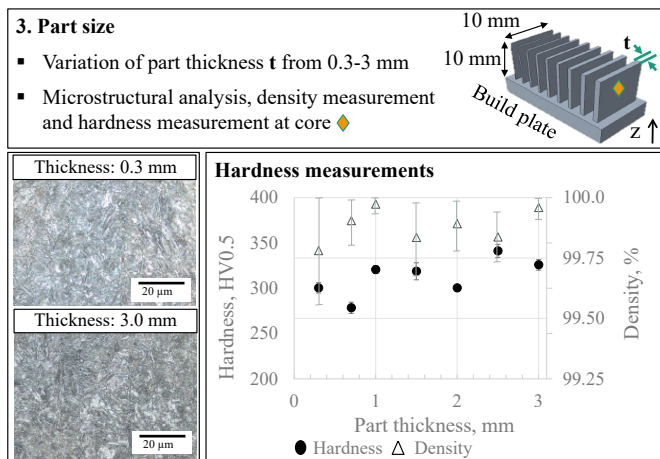
● Hardness △ Density

Fig. 6. Part properties in dependency of the part thickness showing no effect on the hardness measurements and no decrease in density

The effect of overhangs is studied by comparing the microstructure and the hardness of the up-skin and down-skin of specimens built at overhang angles **α** from 30° to 60° (towards the build plate). The results are depicted in Figure 7 showing that there are significant differences between the hardness of up- and down-skin as well as between varied overhang angles. A hardness difference between up- and down-skin of 40 HV0.5 at a 60° overhang angle is measured and increases to 90 HV0.5 at a 30° overhang angle. Additionally, overall hardness is increased by 30 HV0.5 when decreasing the overhang angle to 30°. Microstructure analysis of the down-skin shows an increased ferrite content with increasing overhang angle, which corresponds well with the decreased hardness. It can be concluded that the overhang angle is a key parameter in the heat dissipation process leading to inhomogeneous part properties.

4. Overhang
- Variation of overhang angle **α** from 30° and 60°
- Microstructural analysis and hardness measurement at up-skin (◆) and down-skin (◆)

α = 60°; Down-Skin
α = 30°; Down-Skin

Hardness measurements
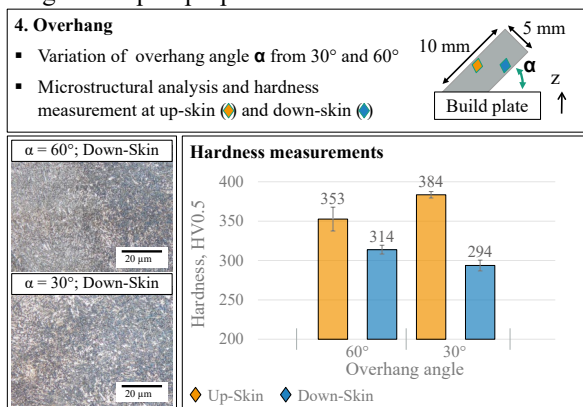
353
314
384
294

◆ Up-Skin ◆ Down-Skin

Fig. 7. Part properties in dependency of the overhang angles showing high dependency of part hardness regarding up- or down-skin measurements

The energy input during solidification of the layer leads to a heat dissipation towards the build plate. One possible principle to influence the occurring heat flux is the change of the cross section area in vertical direction. Within specimens, the ratio from the area **A** and area **B** was varied from 0.05 to 1. Microstructure analysis and hardness measurements were conducted at the core of area **B** (c.f. Figure 8). Measurements show a heat accumulation and reduced heat flux when the ratio is decreased. These effects lead to lower cooling rates and the increased formation of ferrite as the microstructure analysis shows. The hardness values correspond well, showing an increase in hardness by nearly 30 HV2 with increased ratio A/B. Thus, the geometry below a solidified area also has a significant effect in creating inhomogeneous part properties.

5. Vertical cross section
- Variation of cross section **A** to achieve a cross section ratio A/B of 0.05-1
- Microstructural analysis and hardness measurement at core ◆

Ratio A/B: 0.05
Ratio A/B: 1
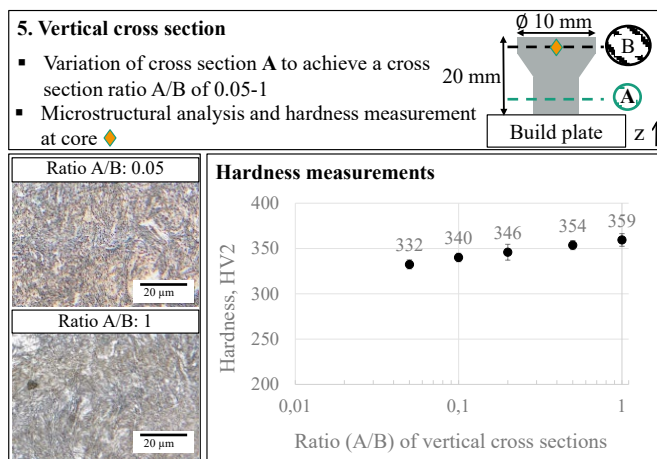
Hardness measurements

332 340 346 354 359

Fig. 8. Part properties in dependency of the cross-section ratio A/B showing an increased ferrite content and decreased hardness with decreasing ratio A/B

To investigate the effect of support structures, parts were built on lattice support with varied support spacing reaching from 0.7 to 2.5 mm (c.f. Figure 9). With lower lattice spacing, the amount of martensite and therefore the hardness increase significantly owing to the higher cooling rates enabled by the heat flux increased by the higher amount of lattice struts. Hardness and microstructure are not affected by an increase in lattice spacing from 1.5 to 2.5 mm. Here, a kind of constant level of heat accumulation seems to be reached which is not decreased by increasing the lattice spacing any further.
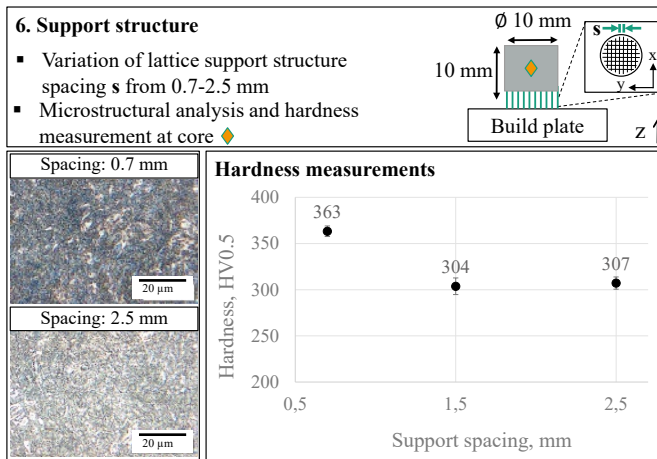
6. Support structure
- Variation of lattice support structure spacing **s** from 0.7-2.5 mm
- Microstructural analysis and hardness measurement at core ◆

Spacing: 0.7 mm
Spacing: 2.5 mm

Hardness measurements

363
304 307

Fig. 9. Part properties in dependency of the applied support lattice spacing showing a high influence of a low spacing distance

4. Mechanical properties depending on the feature size

To determine the dependency of mechanical properties and the feature size, tensile specimen with varied diameter and part thickness were built in vertical direction. At first, the density of all samples was measured (c.f. Figure 10). Comparable results to the "Part size" investigations were obtained.
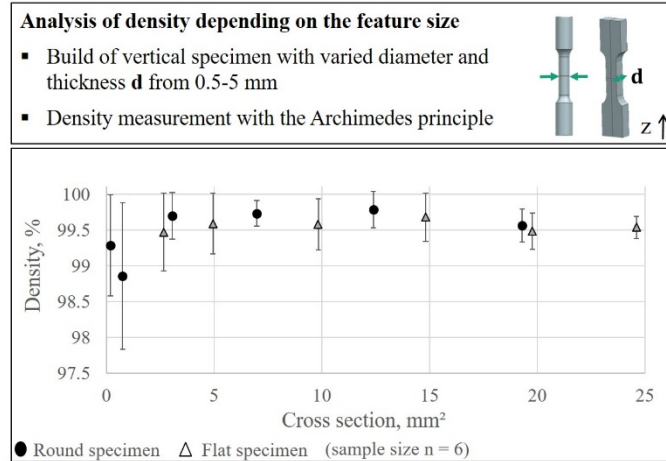

Fig. 10. Part density in dependency of the cross-section size

Since part thickness or respectively diameter were decreased even further the density decreases too. The lowest average densities and highest standard deviations were measured for round specimens at 0.5 mm and 1 mm diameter. Inaccuracies can, however, also be caused by increased surface roughness and powder agglomerates at the overhangs of the specimens. Nevertheless, the influence of feature size is much lower compared to other material groups like titanium or aluminum [13,14]. The resulting tensile strength is displayed in Figure 11 showing constant tensile strength of 1000 N/mm² up to a cross section size of 5 mm². A further decrease in cross section area leads to a decrease in tensile strength until only 60% (626 N/mm²) of the maximum tensile strength (1028 N/mm²) is reached at 0.19 mm² cross section area. A best fit is reached by a logarithmic description of the dependency. Since the variation in the parts' densities is low, the differences can be attributed to the varied ratio of hatch and contour and the ratio of the surface roughness to the cross section.
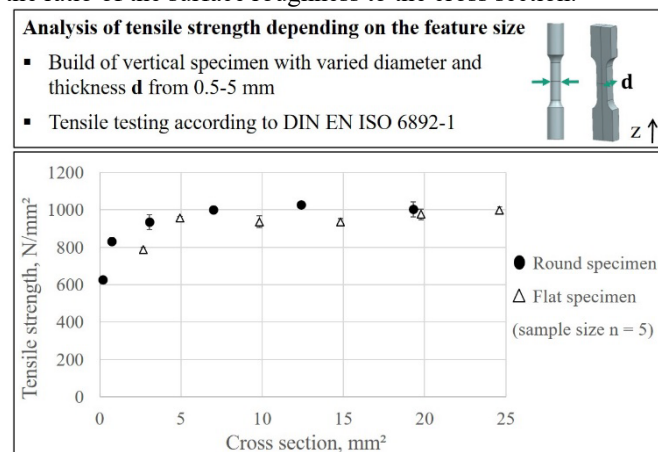

Fig. 11. Tensile strength of the specimens decreases with the decrease of specimen's cross section area

For further insights, scanning electron microscopy images were taken of the fracture surface (c.f. Figure 12). It is obvious that the relation of powder agglomerates at the surface and the cross section decreases with increasing specimen's diameter. Additionally, a more transcrystalline fracture surface is determined at lower diameters, which changes towards a more ductile fracture surface with increasing diameters.
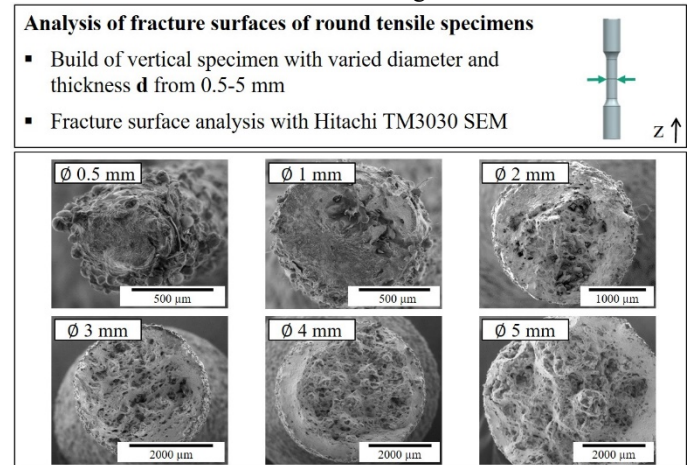

Fig. 12. Fracture surface images of round tensile specimens

5. Discussion

The derived test specimens allowed the identification of main principles influencing the heat dissipation and therefore the microstructure formation in LPBF. Especially changes in the vertical material order like overhangs, cross sections and support structure lead to changes in the heat dissipation. Changes in the horizontal plane (part size and part spacing) lead to insignificant changes. Therefore, it can be concluded that the microstructure is mainly influenced by the heat flow in z-direction. When superpositioning the geometries to one complex part, new effects and interactions might occur which need to be considered in further studies.

The Bal'shin law describes the correlation of properties between bulk and porous material and was derived in the field of powder metallurgy with the porous tensile strength R_m, bulk tensile strength R_{m0}, porous density ρ, bulk density ρ_0 and the Bal'shin exponent m [16]:

$$\frac{R_m}{R_{m0}} = \left(\frac{\rho}{\rho_0}\right)^m. \qquad (1)$$

Applying the Bal'shin law to the data of the tensile specimens leads to a Bal'shin exponent m of 51. Normally, the exponent m lies within a range form 3 to 8 [18]. This indicates that the decrease of tensile strength is not the main contribution of the decreased density. The main factor seems to be the ratio of surface roughness to cross section where the roughness leads to stress concentration effects at the circumference of the specimens. However, the different application (powder metallurgy vs. LPBF) and usually higher porosities used for the Bal'shin law might limit the accuracy.

6. Conclusion and outlook

Following the proposed steps is an effective way to determine the influences of geometric features on the parts microstructure. With the analysis of the derived features, main principles leading to inhomogeneous microstructure and properties can be derived. For the case-hardening steel 16MnCr5 the principles can be divided in three categories by their effect on the resulting microstructure:

No effect: part spacing on the build plate
Low effect: part height and part size
High effect: vertical cross section ratio, overhang angle and support layout.

Furthermore, feature size greatly effects the tensile properties with the ability to decrease tensile strength up to 60%. These findings can be attributed mainly to the roughness and not to the slightly reduced density. Part design and FEA need to consider the size-dependent nature of tensile properties, especially for lattice optimizations.

In further studies, the results of this contribution should be connected to LPBF process simulations to correctly predict the parts' inhomogeneous microstructure and properties.

Acknowledgements

References

[1] M.K. Thompson, G. Moroni, T. Vaneker, G. Fadel, R.I. Campbell, I. Gibson et al., Design for Additive Manufacturing: Trends, opportunities, considerations, and constraints, CIRP Annals 65 (2016) 737–760.

[2] Lutter-Guenther, M., Seidel, S., Kamps, T., Reinhart, G.Lutter-Guenther, M., Seidel, S., Kamps, T., Reinhart, G., Implementation of Additive Manufacturing Business Models, Applied Mechanics and Materials (2015) 547–554.

[3] D. Herzog, V. Seyda, E. Wycisk, C. Emmelmann, Additive manufacturing of metals, Acta Materialia 117 (2016) 371–392.

[4] M. Schmitt, T. Kamps, F. Siglmüller, J. Winkler, G. Schlick, C. Seidel et al., Laser-based powder bed fusion of 16MnCr5 and resulting material properties, Additive Manufacturing 35 (2020) 101372.

[5] M. Schmitt, G. Schlick, C. Seidel, G. Reinhart (Eds.), Examination of the Processability of 16MnCr5 by Means of Laser Powder Bed Fusion, Zeitschrift, Elsevier, 2018.

[6] O. Beer, C. Merklein, D. Gerhard, O. Hentschel, M. Rasch, M. Schmitt, Processing of the Heat Resistant Bearing Steel M50NiL by Selective Laser Melting, Mat.-wiss. u. Werkstofftech. (Materialwissenschaft und Werkstofftechnik 2018 (2018).

[7] D. Bartels, J. Klaffki, I. Pitz, C. Merklein, F. Kostrewa, M. Schmidt, Investigation on the Case-Hardening Behavior of Additively Manufactured 16MnCr5, Metals 10 (2020) 536.

[8] A. Leicht, U. Klement, E. Hryha, Effect of build geometry on the microstructural development of 316L parts produced by additive manufacturing, Materials Characterization 143 (2018) 137–143.

[9] J. Damon, R. Koch, D. Kaiser, G. Graf, S. Dietrich, V. Schulze, Process development and impact of intrinsic heat treatment on the mechanical performance of selective laser melted AISI 4140, Additive Manufacturing 28 (2019) 275–284.

[10] A.v. Müller, G. Schlick, R. Neu, C. Anstätt, T. Klimkait, J. Lee et al., Additive manufacturing of pure tungsten by means of selective laser beam melting with substrate preheating temperatures up to 1000 °C, Nuclear Materials and Energy 19 (2019) 184–188.

[11] G. Mohr, S.J. Altenburg, K. Hilgenberg, Effects of inter layer time and build height on resulting properties of 316L stainless steel processed by laser powder bed fusion, Additive Manufacturing 32 (2020) 101080.

[12] C. Phutela, N.T. Aboulkhair, C.J. Tuck, I. Ashcroft, The Effects of Feature Sizes in Selectively Laser Melted Ti-6Al-4V Parts on the Validity of Optimised Process Parameters, Materials (Basel, Switzerland) 13 (2019).

[13] Z. Dong, X. Zhang, W. Shi, H. Zhou, H. Lei, J. Liang, Study of Size Effect on Microstructure and Mechanical Properties of AlSi10Mg Samples Made by Selective Laser Melting, Materials (Basel, Switzerland) 11 (2018).

[14] T.F. Babuska, K.L. Johnson, T. Verdonik, S.R. Subia, B.A. Krick, D.F. Susan et al., An additive manufacturing design approach to achieving high strength and ductility in traditionally brittle alloys via laser powder bed fusion, Additive Manufacturing 34 (2020) 101187.

[15] D. Barba, C. Alabort, Y.T. Tang, M.J. Viscasillas, R.C. Reed, E. Alabort, On the size and orientation effect in additive manufactured Ti-6Al-4V, Materials & Design 186 (2020) 108235.

[16] M.Y. Bal'shin, Relation of mechanical properties of powder metals and their porosity and the ultimate properties of porous metal-ceramic materials, 1949.

[17] Matthias Schmitt, Deniz Jansen, Andreas Bihlmeir, Jakob Winkler, Christine Anstaett, Georg Schlick et al., Framework and strategies for the lightweight construction of AM gears for the automotive industry, Proceeding RapidTech 2019 (2019).

[18] L. Li, M. Aubertin, A general relationship between porosity and uniaxial strength of engineering materials, Can. J. Civ. Eng. 30 (2003) 644–658.